Article:
Livi, KJT, Villalobos, M, Ramasse, Q orcid.org/0000-0001-7466-2283 et al. (2 more authors) (2023) Surface Site Density of Synthetic Goethites and Its Relationship to Atomic Surface Roughness and Crystal Size. Langmuir: the ACS journal of surfaces and colloids, 39 (1). pp. 556-562. ISSN 0743-7463

https://doi.org/10.1021/acs.langmuir.2c02818

Surface Site Density of Synthetic Goethites and Its Relationship to Atomic Surface Roughness and Crystal Size

Kenneth J. T. Livi,[1] Mario Villalobos[2], Quentin Ramasse[3,4], Rik Brydson[4], Hugo Slavko Salazar-Rivera[2,5]*

1. Department of Materials Science and Engineering, Johns Hopkins University, Baltimore, MD 21218 USA

2. Environmental and Soil Science Dept., LANGEM, Instituto de Geología, Universidad Nacional Autónoma de México (UNAM), CU, CDMX, 04510 México

3. SuperSTEM Laboratory, Keckwick Lane, Daresbury, WA4 4AD UK

4. School of Chemical and Process Engineering, University of Leeds, Leeds LS2 9JT UK

5. Deceased

CORRESPONDING AUTHOR: klivi@jhu.edu

ABSTRACT

The capacity for crystals to adsorb elements and molecules is a function of the structures of their crystal faces and the relative proportions of those faces. More importantly, this study shows that the surface structure of crystal faces is affected by their surface roughness and is the dominant factor controlling absorption site density. In a continuation of the study of synthetic goethites with varying single crystal size distributions, two more synthetic goethites with intermediate sizes were analyzed by BET and atomic resolution STEM to determine the effects of crystal size on their shape, atomic scale surface roughness, and ultimately on their total surface site density. Results show that surface roughness scales directly with the size (or inversely with the specific surface area (SSA)) of synthetic goethite in the SSA range of 40-75 m^2/g. This surface roughness in turn increases the total site density over ideal atomically smooth crystals. The total site density of synthetic goethite increases from a combination of decreasing crystal length:width ratio and increasing surface roughness.

KEYWORDS goethite, adsorption sites, specific surface area, scanning transmission electron microscopy, atomic surface roughness

Introduction

Goethite (α-FeOOH) is a highly abundant and thermodynamically stable Fe(III) oxyhydroxide present in the environment (*1, 2*). It is usually found as colloidal and nano-sized particles and coatings ubiquitous in aqueous environments such as soils and sediments, and in wind-blown mineral dusts (*3, 4*) and influences the transport and fate of numerous aqueous species

through sorptive interactions. Both its bulk and surface structures have been extensively investigated, and the surfaces of ideal goethite crystals have served as a reference for the development of various surface complexation models in current use (*5-8*).

Laboratory preparations of goethite, using the classic Atkinson et al. (*9,10*) synthesis method and small variations thereon, can produce both nanometer- and micrometer-sized particles that have been extensively used for adsorption experiments. In these experiments, the larger particles exhibit higher adsorption capacities than the smaller particles, when normalized by specific surface area (SSA) (as determined by the Brunauer–Emmett–Teller (BET) method using dry preparations (*5-13*)).

Rubasinghege et al. (*14*) have suggested that the nanoparticulate goethite exhibits a greater surface occlusion during particle aggregation under aqueous suspension as compared to the larger micrometer analogs. Indirect quantitative explanations and modeling of this phenomenon were provided by Villalobos and collaborators (*7, 8, 11*) for adsorption of protons, and various cations and anions. They proposed that larger, more reactive, goethites have roughened surfaces as a result of the presence of large proportions of more reactive faces normally found only at the particle tips ({010} and {210} faces). Using the crystallographic reactive site density values of each face, and experimental data of maximum Cr(VI) adsorption for goethites of different particle sizes, they were able to back-calculate the expected fractional contribution of each type of crystal face (for a simple two-crystal face goethite model made of {101}/{010}) to quantitatively describe the adsorption data observed. Fixing these face and site contributions, they successfully modeled the goethite adsorption behavior using surface complexation affinity constants obtained individually for each type of face surface. However, they lacked independent observational data to corroborate their model.

A previous study of two synthetic goethite samples by two of the main authors (*15*) revealed an overall trend of increasing atomic surface roughness with increasing crystal size. In that study, several methods were employed to determine whether size, surface roughness, habit, or oriented attachment in solution were major contributors to changes in absorption capacity. This collection of analyses is time consuming and hence limited the possible number of samples analyzed to two. Therefore, extreme limits of crystal sizes were chosen to represent the overall trend. The study resulted in data for surface area, density, conventional transmission electron microscopy (TEM) observations of crystal lengths and widths, cryo-TEM observation of the state of crystal aggregation in solution versus air-dried samples, electron tomography, and atomic-resolution imaging of crystal perimeters that were gathered and synthesized into model crystals for the two samples.

The picture that emerged for these samples is as follows: The smaller sample (GOE101) had an average crystal length of 107 nm and width of 20 nm, and a large specific surface area (SSA) of 101 m^2/g. Electron tomography revealed that the dominant faces were {101} on the prism and {210} at the tips. An interesting feature of the nanoparticle habit was that one set of the two crystallographically equivalent prism faces was significantly larger than the other, creating a tablet morphology as opposed to rhombic shape in cross section (see Figure 5, Livi et al. (15)). Cryo-TEM imaging showed significant tip-to-tip attachment in solution, but limited prism face attachment. However, electron tomography of air-dried samples showed oriented attachment (OA) configurations of sharing prism faces that foreshadow how aggregation could lead to crystal growth through non-traditional OA pathways.

The larger synthetic sample (GOE42) had an average crystal length of 681 nm and width of 80 nm with an SSA of 42 m^2/g. Cryo-TEM showed that individual crystals were well dispersed

with no tip-to-tip attachments. The larger crystals exhibited the same {101} prism faces but the two crystallographically equivalent prism faces were equant in area.

Conventional TEM data was used to estimate the average crystal habit and crystal face area ratios. The aspect ratios of the two samples were 5.3 and 8.5, for GOE101 and GOE42 samples, respectively. Since the calculated singly-coordinated site density for {210} tip faces (7.5 sites/nm^2) is much higher than the {101} prism face density (3.03 sites/nm^2), a model adsorption site density was calculated based on the relative areas of the two faces. Based on only the ratios of tip-to-prism faces areas, and considering atomically flat crystal faces the calculated site densities of the two samples were 3.31 and 3.36 sites/nm^2 for GOE101 and GOE42 samples. This eliminated the possible cause of changes in site densities between the samples being due to differences in aspect ratio.

Surface roughness was estimated by atomic resolution high-angle annular dark-field scanning TEM (HAADF STEM) and high-resolution TEM (HRTEM) imaging. These methods observed atomic-level steps on the perimeter of goethite prisms and tips and demonstrated that GOE42 was atomically rougher than GOE101. The roughness was determined to arise from the presence of {210}-type steps on the otherwise flat {101} prism faces. GOE101 also showed a certain roughness although to a much lower degree. Since {210}-type steps have a higher site density over {101}-type terraces, the greater the number of steps, the higher the overall site density. Taking into consideration the step proportions of GOE42, the calculated singly-coordinated site density increased to 4.68 sites/nm^2, from the calculated value of 3.36 sites/nm^2 for flat surfaces.

Although the general variation between crystal size and site density for the two extreme-sized goethites was established by Livi et al. (15), the details of the correlation with crystal size could not be established by study of only two samples. Therefore, the current investigation was undertaken to fill in the gap between the crystal size extremes. Here, we investigate two more samples of intermediate sizes and SSA values of 53 and 76 m^2/g and present data from BET, density, TEM and HAADF STEM experiments, to ultimately calculate a more precise trend between BET-SSA and overall crystal face contributions, and thus reactive site densities.

Experimental Section

Sample synthesis

Goethite crystals were synthesized by hydrolyzing Fe(III) solutions with NaOH to pH>12 and aging at 60°C for one day. Experimental details for obtaining sample preparations of different specific surface areas (SSAs), within this protocol are described elsewhere (16). In summary, the crucial experimental parameter used to control the final goethite SSA was the speed of base addition to the Fe(III) solution, being inversely proportional to the resulting SSA. Goethites with values of BET-SSAs of 53 m^2/g and 76 m^2/g were obtained by adding 200 mL of 2.5 M NaOH solution at a rate of 15 mL/min and 7.5 mL/min, respectively to a stirred volume of *ca*. 850 mL of a 60 g/L $Fe(NO_3)_3$ solution (16).

BET measurements

The specific surface area was calculated by the BET method on a Quantachrome Autosorb 1. Before nitrogen adsorption, 200-250 mg of the oven-dried and (mortar-) dispersed goethites were placed on a Quantrachrome 9 mm cell, and outgassed at 105°C for 24 h to remove any

adsorbed water after storage and transport of the goethite. Nitrogen adsorption isotherms were programmed with a 44 data point collection, of which the first 11 were used for SSA calculations.

Specific Gravity (SG) measurements

Picnometers of 10 mL capacity were used, but all volumes were determined gravimetrically. Before use picnometers were carefully washed with a 50% ethanol solution in water and rinsed several times with water. Each picnometer was filled with water to the mark by overflow, carefully paper-drying the overflow, and replicated five times to register an average water-filled weight (W_{p+w}). Goethite samples previously dried at 105 ºC for 12 h were accurately weighed to between 0.3 and 0.4 g inside the picnometers (W_g) and were half-filled with water, in triplicates per each goethite. These were ultrasonicated for 1 h and subsequently were left stationary to let solids settle towards the bottom of the picnometer. Additional water was added to reach the lower part of the narrow neck of the picnometer taking care not to disturb the underlying suspension, the lid was placed and any water overflow was paper-dried off. The total weight was computed (W_{p+w+g}). Assuming a water density of 1 g/cm^3, the calculations performed were:

$$\text{Goethite SG} = (W_g)/(W_g+W_{p+w}-W_{p+w+g})$$

TEM and STEM Sample Preparation

A small portion of the crystals were suspended in double-distilled deionized water and ultrasonicated for 3 minutes. A TEM grid covered with ultrathin carbon film on lacey-carbon support film was dipped immediately into the goethite suspension and allowed to dry. Examination of the air-dried samples was initially performed on a Philips CM 300 FEG TEM at 300 kV at Johns Hopkins University. Since the 300 kV beam is capable of damaging the goethite structure, care was taken not to damage the smallest crystals by performing low-dose procedures.

Aberration-Corrected Stem HAADF Conditions

HAADF-STEM imaging was carried out on a dedicated aberration-corrected Nion UltraSTEM 100 STEM, operated at 100 kV. The microscope electron optics were configured to form a probe of 30 mrad half-angle convergence with 30pA beam current, resulting in a 0.1 nm probe size. The HAADF detector angular range was calibrated as 85-190 mrad.

Image processing

STEM HAADF images of crystal perimeters were acquired as stacks of rapid scans of approximately 25 elongated frames of 512 pixels x 1024 pixels (the longer image side being aligned with that of the lath-shaped crystals) at 2.5μs/pixels (resulting in a rate of 1.3 frames per second) and with a pixel size of 0.03nm. In order to mitigate possible damage to the structure at the surface of the nanocrystals under the electron beam, great care was taken to set up the imaging conditions and parameters away from the regions of interest, and only acquiring one single image stack of a given area prior to shifting the scanned area along the crystal perimeter, ensuring only fully pristine surface structures were examined.

Raw image stacks were aligned and filtered using the routine described in reference (17). The rigid registration algorithm used a Butterworth Low Pass filter for noise reduction and a Hanning Window High Pass filter for edge detection. This sped up the alignment of image stacks and the detection of the last Fe atom without introducing a frequency filter that could extend periodicity of the lattice into the noise of the amorphous carbon that was always found at the edge of the crystals. However, the resulting image flattening procedure does cause intensities to fluctuate into negative values. Careful comparisons of last atom detection in filtered and unfiltered images showed that there were no significant differences in the surface roughness measurements. A comparison between a pair of filtered and unfiltered images is provided in the Supplementary Information Figure S1 for reference.

Results and Discussion

BET and Mass Density measurements

Results of BET and density of goethite samples are presented in Table 1.

Table 1. Experimental goethite characterization parameters.

Goethite sample	Specific Surface Area[a] (m^2/g)	Mass density[b] (g/cm^3)
GOE76	76 ±3	3.46 ±0.01
GOE53	53 ±3	3.34 ±0.01

[a] From nitrogen adsorption BET measurements

[b] From 3 replicates

Crystal Habit and Size

The crystal habits of GOE76 and GOE53 were investigated by conventional TEM imaging. From TEM images of crystals prepared by air-dried methods, goethite particles of both samples crystallized as laths that were elongated along the **b**-axis (*Pnma* setting)(Fig. 1). The average dimensions of crystal lengths and widths for both samples are given in Table 2. Samples GOE53 and GE76 had similar length:width ratios, 9 and 7.1 respectively, and were comparable with the range found for GOE42 and GOE101 (8.5 and 5.3 respectively).

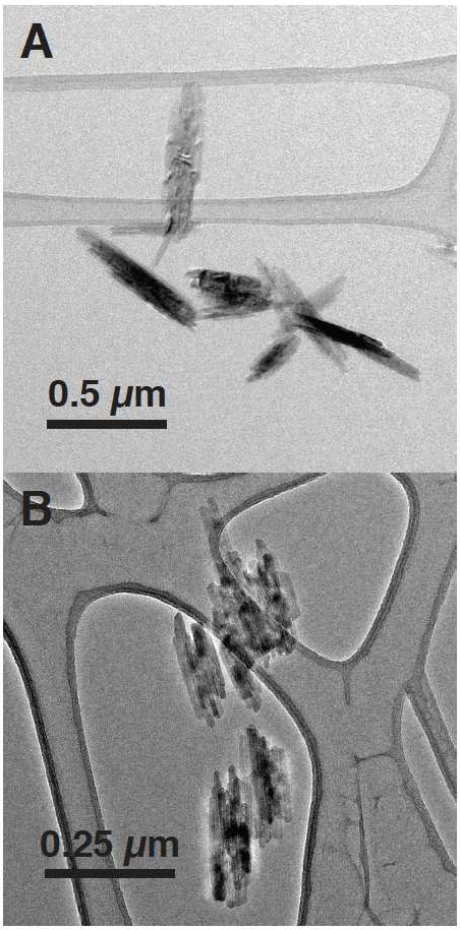

Figure 1. Conventional TEM images of air-dried GOE53 (A) and GOE76 (B). Note the change in scale and the amount of clustering of particles in both samples.

Table 2. TEM measurements of crystal dimensions.

Sample	GOE76	GOE53
Length (nm)	205	720
St Dev (1s)	64	177
Error of Mean	9	42
Min	67	335
Max	454	1087
Width (nm)	29	80
St Dev (1s)	23	42
Error of Mean	3	10
Min	9	18
Max	125	150
L:W	7.1	9

Histograms for the lengths (L) and widths (W) of several synthetic goethites are presented in Figure 2. Since all samples have average length:width ratios close to 10, the lengths and widths curve centroids plot near each other for each goethite. For all samples except SSA=42, the histograms for both L and W are skewed to shorter values. It is also important to note that as the SSA decreases, the width of the distributions for both L and W increases. This most likely reflects the non-classical growth process of oriented attachment (18-20).

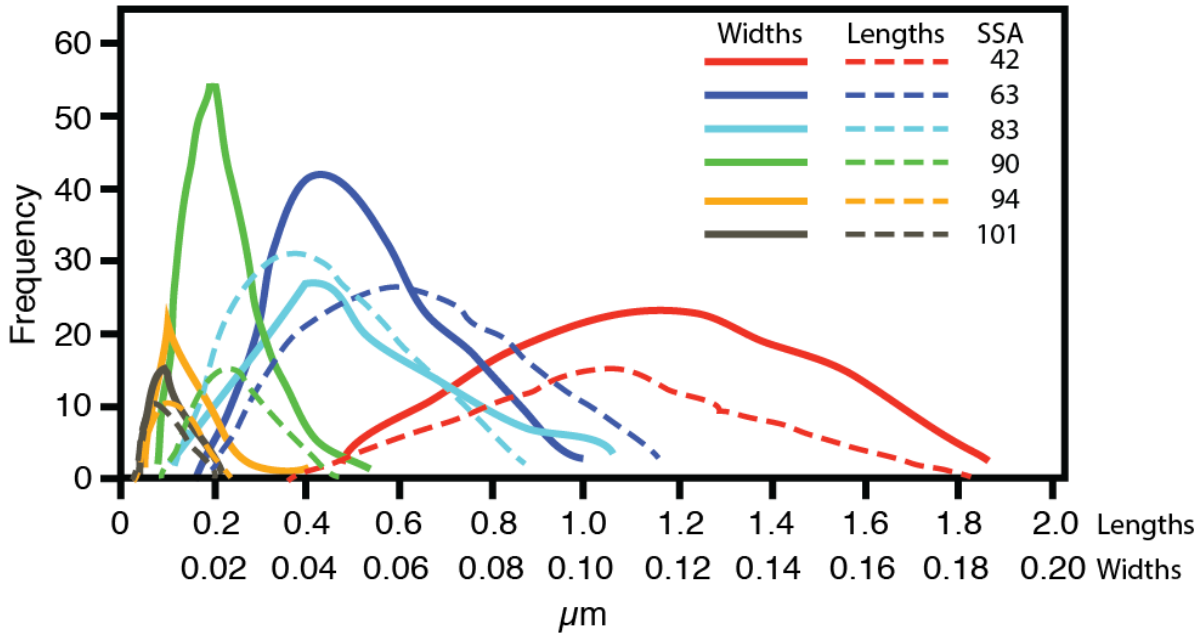

Figure 2. Widths and lengths of several synthetic goethite samples versus frequency of occurrence (number of crystals). Solid lines = widths, dotted lines = lengths.

In these air-dried drop-cast samples, the smaller crystals tend to attach by sharing prism faces, while the larger crystals tend to share tips. This is similar to previous findings (15) for air-dried preparations. However, cryo-TEM preparation of GOE101 revealed a strong tendency for tip-to-tip attachment whilst in solution (15).

STEM imaging

Goethite particles were imaged down the [001] axis, which aligned and separated oxygen atom columns from iron atom columns in the structure. In this orientation, atomic-resolution STEM HAADF resolved individual Fe atom columns and revealed the atomic-scale morphology of the goethite crystal perimeter (Fig. 3a). From these images, the atomic roughness of the perimeter can be directly measured by counting Fe pairs parallel to the {101} prism faces and pairs

parallel to {210} steps. This followed the procedure described by Livi et al. (21). An illustration of how the perimeter atom was determined is shown in Figures 3b-3e. In 3b, the prism edge is imaged down [001]. Four profiles, 5 pixels wide, are then drawn at the edge of the prism (Fig 3c). The intersection of the profiles is marked by red boxes in 3d. All four profiles are moved together and when the three white profiles locate the final peak above background in the red boxes, that atom is labeled with a red circle in (E). For every Fe-atom pair, a step orientation is then assigned (Fig 3e).

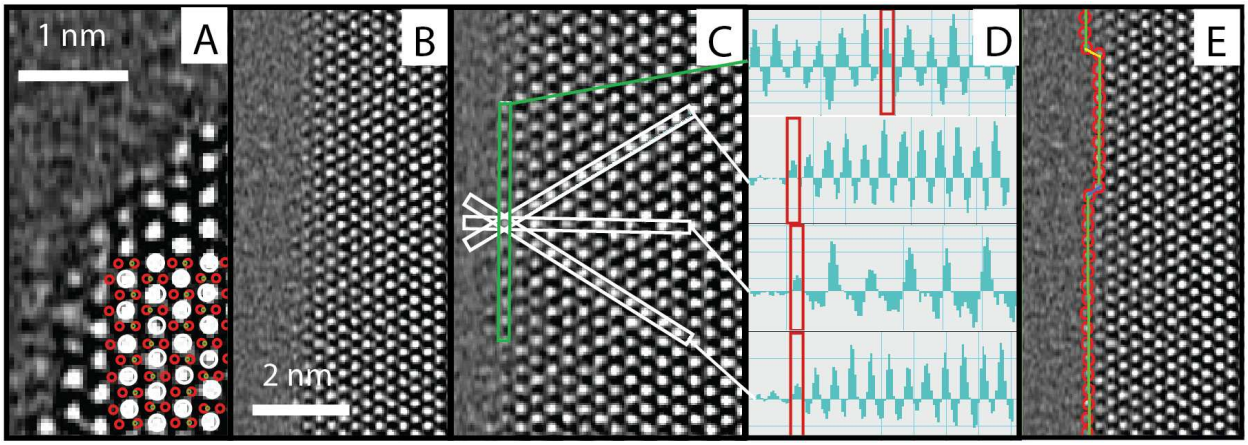

Figure 3. (A) AC-STEM HAADF image of the {101} prism – {210} tip perimeter. White dots (with white circles) represent the Fe-atom column positions looking down the [001] direction and the red circles locate oxygen atoms positions. (B). A HAADF image of a {101} prism. (C) Four profiles drawn to determine last atom position. (D) Profile intensities - intensities go negative due to the statistically determined spatial drift filters. (E) location of last Fe atom position.

Images of tips and sides for the two samples are given in Figure 4 along with the perimeter assignment. Over one thousand Fe-pairs were counted for two crystals each for the two samples and results are presented in Table 3. The STEM results showed that there was a significant

proportion of {210} steps present on the crystal prism faces for both samples. If steps observed at the perimeter are the final expression of steps found on the faces of goethite crystals, then perimeter roughness measurements are faithful estimates of the total surface atomic roughness.

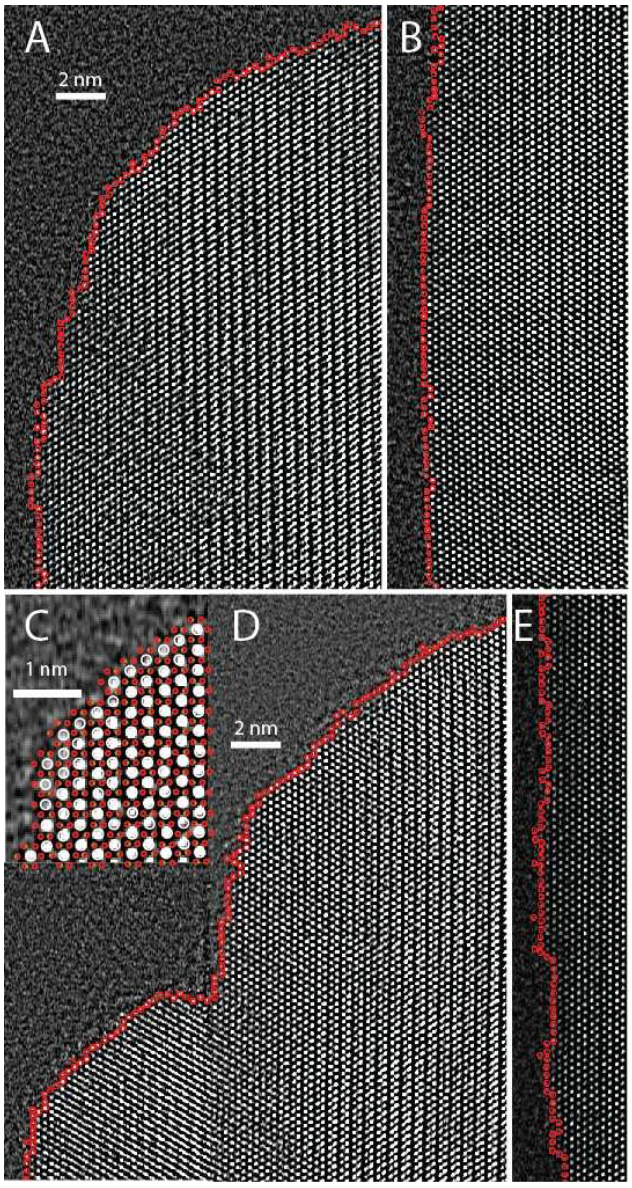

Figure 4. (A) {101}-{210} corner and (B) {101} prism of GOE76. (C) Detail of GOE53 corner. (D) {210} tip and (E) {101} prism of GOE53.

Table 3. Surface Step proportions on particle surfaces of GOE76 and GOE53

Sample	Step Type	Percent of Prism	Percent of Tip
GOE76	{101}	76 ± 2	26 ± 1
	{210}	24 ± 0.5	74 ± 4
	{001}	0	0
GOE53	{101}	70 ± 5	16 ± 1
	{210}	30 ± 1	84 ± 1
	{001}	0	0

Model Specific surface areas and SIte Densities

Ideal Model

Each individual crystal measured by conventional TEM had a full surface area model calculated based on simple geometric relationships related to the angle between the {101} and {210} faces and the width and length of crystals. The averages of all calculated crystal properties are presented in Table 4 and designated as the Ideal Model. **This model does not account for surface roughness.**

Table 4. Calculated Surface areas and Volumes of single crystals based on conventional TEM measurements.

Sample	Faces Present	Ideal Face Area ($x10^4$ nm^2)	Ideal Total Surface Area ($x10^4 nm^2$)	Ideal Vol ($x10^4 nm^3$)	Ideal Model SSA (m^2/g)
GOE76	{101}	1.24 ± 0.01	1.33 ± 0.01	3.7± 0.5	101 ± 2
	{210}	0.092 ± 0.001			
GOE53	{101}	12.2 ± 1.5	12.9 ± 1.6	102± 51	39 ± 2
	{210}	0.70 ± 0.14			

The ideal site densities were then calculated from the Ideal Model surface areas assuming atomically flat faces (Table 5). In the Ideal Model, the prism faces only contain {101}-type sites, for which crystallographic analyses show a site density of singly-coordinated sites of 3.03 sites/nm^2 (*12*), and the tip faces only have {210}-type sites with an areal density of 7.5 singly-coordinated sites/nm^2. As expected, based simply on the TEM measurements, ideal crystal geometry and atomically smooth faces, the calculated site densities for GOE53 and GOE76 are not very different from each other (3.27 versus 3.34 sites/nm^2), which reflects the fact that the L:W aspect ratios of GOE53 and GOE76 are not very different. The calculated effect of changing length:width ratios on the singly-coordinated site densities of ideal crystals is shown in Figure S2. It is important to note that the ideal singly-coordinated site density is relatively constant at 3.2 sites/nm^2 when the L:W ratio is 10 or greater, but increases significantly when the L:W decreases below 5.

Table 5. Calculated reactive singly-coordinated surface sites based on TEM measurements.

Sample	Faces	Ideal Model Sites (x10^4)	Ideal Model site density (#/nm^2)
GOE76	{101}	3.76 ± 0.40	3.34 ± 0.01
	{210}	0.69 ± 0.07	
GOE53	{101}	36.0 ± 4.4	3.27 ± 0.01
	{210}	5.27 ± 1.1	

Surface Roughness Model

When taking into account surface roughness (SR Model) (Table 6), the total proportions of {101} and {210} type sites, regardless of whether they are found on the prism or tip faces, are considered. In the SR Model, both GOE53 and GOE76 increase in terms of estimated site density and are intermediate between GOE42 and GOE101. These are considered the best estimates of the true singly-coordinated site densities of the synthetic goethites produced by the classic Atkinson et al. (*9,10*) method.

Table 6. Calculated reactive singly-coordinated surface sites based on the surface roughness measurements.

Sample	Faces	SR Model Sites ($x10^4$)	**SR Model site density (#/nm^2)**
GOE76	{101}	5.09 ± 0.46	**4.26 ± 0.08**
	{210}	0.58 ± 0.06	
GOE53	{101}	53.3 ± 6.6	**4.50 ± 0.02**
	{210}	4.77 ± 0.95	

Summary of Existing Data

Crystal Size Data

The different sets of data gathered here for synthetic goethite particles of different SSAs show some interesting trends. The most dramatic one is that observed in Figure 2, where a large increase in the range of particle size distributions was observed as SSA decreased, with extensive overlaps among different goethite preparations. This is especially evident in the case of the 42

m^2/g goethite, for which individual particle lengths varied from 0.4 mm to 1.8 mm, with a near-Gaussian distribution centered around *ca*. 1.1 mm. This would evidently translate to a similarly wide distribution of SSAs for this goethite. However, from the perspective of modeling their adsorption behavior, it is difficult to incorporate these variations, because it is the average SSA values that are measured and utilized. The average length/width ratios also increased as SSA decreased, but to a lower extent, from *ca*. 5 to 8.5-9 for the largest goethites, *i.e*., the particles tend to elongate as they become larger. Fortunately, this L:W range is where the aspect ratio has a little effect on the site density of goethite.

Surface Roughness Data

The most important conclusion of this study is that the goethite surface roughness increases as particle size increases, mostly on the prism side of the crystals. This is shown in Figure 5a as an increasing total contribution of {210} steps that appear on the {101} tablet habit.

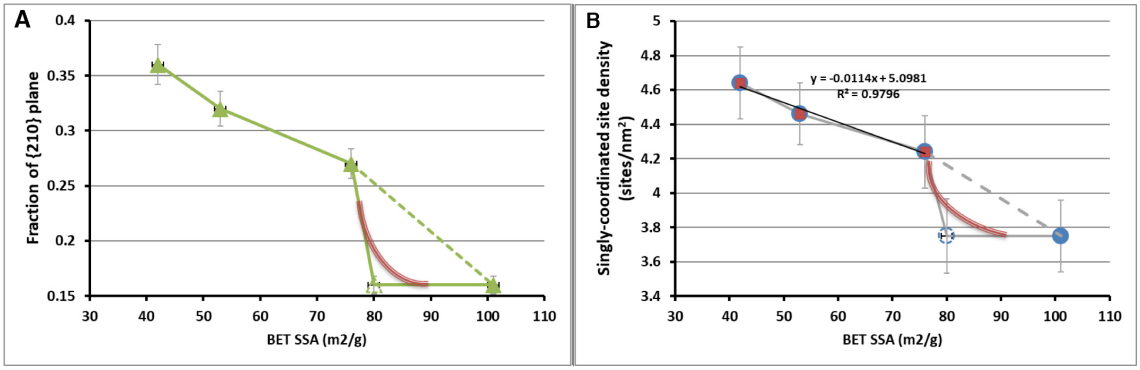

Figure 5. Surface roughness variation as a function of SSA (BET), shown as: (a) total contributions of the {210} face, and as; (b) resulting reactive site densities of singly-coordinated sites (calculated from the reactive sites on each face estimated by (22)). Error bars for the latter are ±0.21 sites/nm^2. The data for 42 m^2/g and 101 m^2/g goethites were taken from (15). The

discontinued line shows the data-suggested trend between the highest SSA goethite measured (110 m^2/g) and the next studied goethite of 76 m^2/g, while the full and shaded red lines show more probable scenarios based on evidence described in the text.

Both the {210} face fraction contribution, and, especially, the corresponding reactive singly-coordinated surface site density, exhibit near linear relationships with the BET SSA in the range 42 to 76 m^2/g. This trend is encouraging because it suggests that the corresponding values for other goethites within this SSA range may easily be estimated from the regression line. The behavior is less clear for SSA greater than 76 m^2/g because only one sample, 101 m^2/g, has been rigorously analyzed by the suite of electron microscopy techniques described in the present work, and it would be tempting to interpolate a straight line between them (discontinued lines in Fig. 5). This line only deviates slightly from the regression line calculated for the lower SSA range, so a compelling argument could be made about this interpolation being correct.

However, previous experimental evidence shows that goethites of 80 m^2/g and of 105 m^2/g SSA show equal phosphate adsorption maxima of 2.4-2.5 $\mu mol/m^2$ (23) and (24), respectively; as compared to goethites of much lower SSAs of 28-38 m^2/g, showing maxima of 2.8 to 5.4 $\mu mol/m^2$ (22-24). Also, proton adsorption data obtained in our laboratory showed overlapping charging curves at three different ionic strengths for an 82 m^2/g goethite and a 94 m^2/g goethite (*cf.* Fig S3). These data and low adsorption maxima of other anions, such as citrate and selenite for goethites of 80-81 m^2/g (23, 25) suggest that goethite samples of 80 m^2/g and above behave in a similar manner, and thus show the same reactive surface site densities. For this reason, a flat horizontal line in this SSA range has been plotted as a probable behavior for goethite in Figure 5. It is also

possible that there is also an increase in surface site density as the SSA decreases in this range, but that the correlation line follows a gentler slope, such as the curved behavior suggested in Figure 5, in which these differences are not reflected in differences in adsorption capacities in this range; although it is difficult to justify that a decrease in total reactive site density would not have a highly sensitive effect on the maximum adsorption of ions on goethite. In either case, a very large increase in site density is expected to occur in the very short SSA range between 80 and 76 m^2/g. This needs to be further investigated by studying goethites within this narrow SSA range.

Applicability to Natural Systems

A criticism of this and previous studies (15) could be made in that the synthetic crystals studied are not representative of natural systems. Although that is true, natural systems tend to be more heterogeneous than controlled experiments. The data examined here unequivocally explain the reasons for the changes in site densities of synthetic samples produced by the most accepted method of synthesizing goethites of different sizes. In lieu of studies that compare the crystal size distribution, surface roughness, and site densities of natural samples with synthetic samples, the prediction of site densities presented here are the best estimates yet. Further in-depth studies of carefully selected natural samples are needed to determine the confidence of applying our conclusions to natural systems.

Additionally, the crystal face contributions measured in this work for different goethites may be used in further studies to determine unified proton and ion affinity constants from adsorption experiments. Typically, protons are assumed to be reactive to singly- and triply-coordinated surface sites, whereas ions are normally modeled as reactive only towards singly-coordinated surface sites. The affinity constants found should be applicable to any goethite (synthetic or natural) because they are independent of its particular site density value.

Conclusion

Extending the previous study of Livi et al. (15), we have strengthened the conclusion that surface roughness is the dominant cause for changes in site densities as particle sizes of goethites increase when synthesized by the Atkinson et al. (*9,10*) method. Figure 5 can be used to estimate the site capacities for similar synthetic goethites in adsorption experiments. These observations dictate that particle aspect ratio alone cannot be used to predict the site density of goethite samples. Some form of TEM observation must be performed to determine the extent of surface roughness. This is most effectively done on aberration-corrected (S)TEMs which are beginning to become more readily available.

Acknowledgements

K.J.T.L., M.V. and H.S. S.-R. would like to acknowledge funds provided by CONACyT Ciencia Básica 2016 project number 283416; and would also thank the assistance of Ulises Loredo-Jasso in measuring goethite crystal mass densities. H.S. S.-R. is grateful to CONACyT for the Ph.D. student fellowship received. We acknowledge V. Maturano and the Physics Institute at UNAM for technical support in BET measurements. Funds granted to the LANGEM by the UNAM are also highly appreciated. SuperSTEM is the UK National Research Facility for Advanced Electron Microscopy, supported by the Engineering and Physical Sciences Research Council (grant reference EP/W021080/1).

Supporting Information Available:

Illustration of method of image processing

Calculated relationship of bulk singly-coordinated site densities of ideal goethite crystals with changing aspect ratios

Surface proton behavior at different ionic strengths

Table of calculated site densities

This material is available free of charge via the Internet at http://pubs.acs.org.

References

(1) Bigham, J. M.; Fitzpatrick, R. W.; Schulze, D. G. Iron oxides. In *Soil mineralogy with environmental applications. SSSA Book Series no. 7* (eds. J.B. Dixon and D.G. Schulze). *Soil Science Society of America, Madison, Wisconsin* **2002**, pp. 323-366.

(2) Langmuir, D. Aqueous Environmental Geochemistry. *Prentice Hall, USA,* **1997**.

(3) Waychunas, G. A.; Kim, C. S.; Banfield, J. F. Nanoparticulate iron oxide minerals in soils and sediments: unique properties and contaminant scavenging mechanisms. *Journal of Nanoparticle Research* **2005**, *7*, 409-433.

(4) Raiswell, R. Iron Transport from the Continents to the Open Ocean: The Aging–Rejuvenation Cycle. *Elements* **2011**, *7*, 101-106.

(5) Hiemstra, T.; Van Riemsdijk, W. H. A surface structural approach to ion adsorption: the charge distribution (CD) model. *J. Colloid Interface Sci.* **1996**, *179*, 488-508.

(6) Hiemstra, T.; Van Riemsdijk, W. H. Fluoride adsorption on goethite in relation to different types of surface sites. *J. Colloid Interface Sci.* **2000**, *225*, 94-104.

(7) Villalobos, M.; Cheney, M. A.; Alcaraz-Cienfuegos, J., Goethite surface reactivity: II. A microscopic site-density model that describes its surface area/normalized variability. *J. Colloid Interface Sci.* **2009**, *336*, 412-422.

(8) Salazar-Camacho, C.; Villalobos, M. Goethite surface reactivity: III. Unifying arsenate adsorption behavior through a variable crystal face – Site density model. *Geochimica et Cosmochimica Acta* **2010**, *74*, 2257-2280.

(9) Schwertmann, U.; Cornell, R.M. *Iron oxides in the laboratory – Preparation and characterization*. WILEY-VCH Verlag GmbH, D-69469 Weinheim Germany **2000**, p. 204.

(10) Atkinson, F..J.; Posner, A. M.; Quirk, J. P. Adsorption of Potential-Determining Ions at Ferric Oxide-Aqueous Electrolyte Interface. *J. Phys. Chem.* **1967**, *71*, 550.

(11) Villalobos, M.; Trotz, M.; & Leckie, J. O. Variability in goethite surface site density: Evidence from proton and carbonate sorption. *J. Colloid Interface Sci.* **2003**, *268*, 273-287.

(12) Cwiertny, D. M.; Hunter, G. J.; Pettibone, J. M.; Scherer, M. M.; Grassian, V. H. Surface chemistry and dissolution of α-FeOOH nanorods and microrods: Environmental implications of size-dependent interactions with oxalate. *J. Phys. Chem. C*. **2009**, *113*, 2175-2186.

(13) Wijenayaka, L. A.; Rubasinghege, G.; Baltrusaitis, J.; Grassian, V. H. (2012) Surface Chemistry of α-FeOOH Nanorods and Microrods with Gas-Phase Nitric Acid and Water Vapor: Insights into the Role of Particle Size, Surface Structure, and Surface Hydroxyl Groups in the Adsorption and Reactivity of α-FeOOH with Atmospheric Gases. *J. Phys. Chem. C* **2012**, *116*, 12566−12577.

(14) Rubasinghege, G.; Kyei, P. K.; Scherer, M. M.; Grassian, V. H. Proton-promoted dissolution of α-FeOOH nanorods and microrods: Size dependence, anion effects (carbonate and phosphate), aggregation and surface adsorption. *J. Coll. Interface Sci.* **2012**, *385*, 15–23.

(15) Livi, K. J. T.; Villalobos, M.; Leary, R.; Varela, M.; Barnard, J.; Villacís-García, M.; Zanella, R.; Goodridge, A.; Midgley, P. Crystal face distributions and surface site densities of two synthetic goethites: Implications for adsorption capacities as a function of particle size. *Langmuir*, **2017**, 33, 8924-8932, 10.1021/acs.langmuir.7b01814.

(16) Villacís-García, M.; Ugalde-Arzate, M.; Vaca-Escobar, K.; Villalobos, M.; Zanella, R.; and Martínez-Villegas N. (2015) Laboratory synthesis of goethite and ferrihydrite of controlled particle sizes. *Boletín de la Sociedad Geológica Mexicana* **2015**, 67(3), 433-446.

(17) Schaffer, B., Grogger, W., Kothleitner, G. Automated Spatial Drift Correction for EFTEM Image Series. *Ultramicroscopy*, **2004**, *102*, 27-36.

(18) Penn, R.; Banfield, J. Oriented attachment and growth, twinning, polytypism, and formation of metastable phases: Insights from nanocrystalline TiO_2. *American Mineralogist* **2015**, *83*, 1077-1082.

(19) De Yoreo, J.J.; Gilbert, P.U.P.A; Sommerdijk, N.A.J.M.; Penn, R.L.; Whitelam,S.; Joester, D.; Zhang, H.; Rimer, J.D.; Navrotsky, A.; Banfield, J.; Wallace, A.F.; Michel, F.M.; Meldrum, F.C.; Cölfen, H.; Dove, P.M. Crystallization by particle attachment in synthetic, biogenic, and geologic environments. *Science* **2015**, *349*, 6247, DOI: 10.1126/science.aaa6760.

(20) Yuwono, V.M.; Burrows, N.D.; Soltis, J.A.; Penn, R.L. Oriented aggregation: Formation and transformation of mesocrystal intermediates revealed. *J. Am. Chem. Soc.* **2010**, *132*, 2163–2165.

(21) Livi, K. J. T.; Schaffer, B.; Azzolini, D.; Sverjensky, D.; Hazen, R.; Brydson, R. Atomic-scale surface roughness of rutile and implications for organic molecule adsorption. *Langmuir* **2013**, *29*, 6876-6883.

(22) Venema, P., Hiemstra, T., Van Riemsdijk, W.H., Multisite adsorption of cadmium on goethite, *J. Colloid Interface Sci.* **1996**, *183*, 515.

(23) Bowden, J.W., Nagarajah, S., Barrow, N.J., Posner, A.M., Quirk, J.P. Describing the adsorption of phosphate, citrate and selenite on a variable-charge mineral surface, *Aust. J. Soil Res.,* **1980**, *18***,** 49-60.

(24) Hiemstra, T., Van Riemsdijk, W.H. A Surface Structural Approach to Ion Adsorption: The Charge Distribution (CD) Model, 1996, *J. Colloid Interface Sci.*, **179,** 488-508.

(25) Hingston, F.J., Posner, A.M.; Quirk, J.P. Anion adsorption by goethite and gibbsite: I. The role of the proton in determining adsorption envelopes, *J. Soil Sci.*, **1972** 23, 177–192.

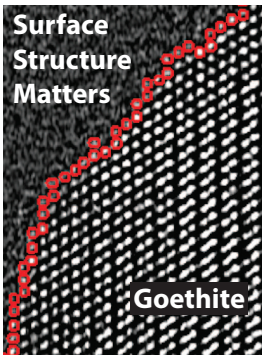

TOC Art